



A robust Zr(IV)-based metal-organic framework featuring high-density free carboxylic groups for efficient uranium recovery

Bin Wang^{a,b,c}, Chunyu Bao^a, Jiahui Xu^a, Yunnan Tao^a, Long Chen^a, Duo Zhang^a, Kui Tan^c, Shuao Wang^{a,*}, Jian-Rong Li^{b,*}, Shengqian Ma^{c,*}

^a State Key Laboratory of Radiation Medicine and Protection, School for Radiological and Interdisciplinary Sciences (RAD-X), and Collaborative Innovation Center of Radiation Medicine of Jiangsu Higher Education Institutions, Soochow University, Suzhou 215123, China

^b Beijing Key Laboratory for Green Catalysis and Separation and Department of Chemistry and Chemical Engineering, College of Environmental and Energy Engineering, Beijing University of Technology, Beijing 100124, China

^c Department of Chemistry, University of North Texas 1508W Mulberry St, Denton, TX 76201, USA

ARTICLE INFO

Keywords:

Uranium
Metal-organic framework
Carboxylic group
Radioactive management

ABSTRACT

The extraction of uranium from aqueous environments, including the ocean and radioactive wastewater, represents a significant challenge with profound implications for energy resources and environmental remediation. This work presents the design and synthesis of a novel highly stable carboxylated metal-organic framework, BUT-12-3COOH, which achieves excellent U(VI) extraction ability from water. BUT-12-3COOH features high-density free carboxylic groups, exceptional chemical stability, fast kinetics, and high adsorption capacity for U(VI). Dynamic sorption experiments further demonstrated the potential of BUT-12-3COOH in treating real radioactive wastewater. The mechanisms for the U(VI) capture of BUT-12-3COOH are investigated through the combination of EDS, FT-IR, and XPS analysis. The results of this study underscore the promising utility of BUT-12-3COOH as an effective sorbent for extracting radionuclides from environmental specimens and liquid nuclear waste streams.

1. Introduction

The exponential rise in human population and industrial activities has precipitated a marked depletion of global petrochemical fuel reserves, coupled with an uptick in greenhouse gas emissions. This critical scenario underscores the imperative for an immediate investigation into sustainable and environmentally benign alternative energy sources. Nuclear power stands out as a green energy option due to its high efficiency in electricity generation and minimal greenhouse gas emissions [1]. However, the constrained supply of nuclear fuel resources represents a salient impediment to the accelerated deployment of nuclear energy [2]. Uranium, the essential strategic nuclear power resource, is found in terrestrial ores with reserves of only about 6.3 million tons. The ocean contains an enormous amount of uranium, accounting for 99.9 % of the total uranium found on Earth, which adds up to a staggering 4.5 billion tons. Yet, the paltry concentration of uranium in seawater, a mere 3.3 parts per billion (ppb), alongside the presence of copious competing ions, presents a formidable extraction challenge [3]. Additionally, extracting uranium from spent fuel, which contains a significant amount

of unreacted uranium, during the reprocessing process is also a challenge. One crucial aspect of tackling these challenges involves the creation of novel adsorbent materials that possess exceptional chemical stability and demonstrate specific and efficient capabilities for capturing U(VI) ions in both seawater and radioactive water [4–22].

Over the past two decades, metal-organic frameworks (MOFs), a class of inorganic-organic hybrid materials constructed from the coordination of metal centers and organic linkers, have garnered immense attention for their intriguing architectures as well as their vast potential applications such as gas storage [23,24], gas separation [25], heterogeneous catalysis [26,27], proton and/or electron conduction [28,29], degradation of chemical warfare agents [30,31], food safety [32], sensing [33], enantioselective separation [34], and so on. Particularly, the remarkable design flexibility of MOFs enables the incorporation of functional groups with precise binding sites for guest molecules within the pores of MOFs, achieved through pre-linker or metal node design, as well as post-synthesis modification approaches [35]. This ability allows MOFs to effectively and specifically capture targeted substances. These methods have been employed to develop MOF-based sorbents that

* Corresponding authors.

E-mail addresses: shuao.wang@suda.edu.cn (S. Wang), jrl@bjut.edu.cn (J.-R. Li), shengqian.ma@unt.edu (S. Ma).

<https://doi.org/10.1016/j.cej.2024.150251>

effectively capture U(VI) from seawater or radioactive wastewater [36,37]. For instance, we successfully incorporated amidoxime (AO), the highly effective functional group for uranium extraction, into the pores of UiO-66 for the first time. The obtained functional MOF, UiO-66-AO, demonstrated selective capture of U(VI) from seawater with a sorption capacity of 2.68 mg/g in real seawater [38]. Following a similar approach, AO was introduced into other MOFs, such as MIL-53 and ZIF-90, to extract uranium from seawater [39,40]. Despite the promising extraction performance of AO-functionalized MOFs for U(VI), the current methods for synthesizing these materials typically involve a two-step post-synthetic modification process. In this process, the $-\text{CN}$ functional group is first introduced to the pores of MOFs and then converted into AO [38]. The density of AO groups achieved through this approach is thus relatively low, which hinders the full potential development of the material. In addition to AO, the introduction of other functional groups such as $-\text{OH}$ [41,42], $-\text{NH}_2$ [43–46], $-\text{COOH}$ [47], and $-\text{H}_2\text{PO}_4$ [48–51] can also enhance the adsorption capacity of the functional MOFs for U(VI). Among these groups, carboxyl group-functionalized MOFs are considered excellent materials for capturing U(VI) due to the relative strong coordination ability of carboxylic group with U(VI). Furthermore, $-\text{COOH}$ can be introduced into the ligands of MOFs through rational structural design to maximize their density in the pores, thereby increasing the adsorption capacity for U(VI). Zhao et al. studied the adsorption performance of two reported carboxylated MOFs, UiO-66-COOH and UiO-66-2COOH, for U(VI) sorption. The results showed that UiO-66-2COOH with a higher carboxyl density exhibited superior U(VI) adsorption performance [47]. Therefore, it is reasonable to believe that constructing MOFs with high carboxyl density is an effective strategy to improve U(VI) adsorption capacity. Additionally, the chemical stability of the MOFs is an important prerequisite for the extraction of U(VI) from seawater or radioactive water, and MOFs containing high-valence metal ions including Zr^{4+} , Al^{3+} , and Cr^{3+} usually exhibit excellent chemical stability [52].

In the previous work, we reported an excellent chemically stable Zr (IV)-based MOF, BUT-12, prepared by reacting a tritopic carboxylic acid ligand named H_3CTTA with ZrCl_4 in N,N -dimethylformamide (DMF, Fig. 1b,d). The distinctive feature of the ligand used in the construction

of BUT-12 is the presence of three methyl groups attached to the central benzene ring (Fig. 1b). These methyl groups introduce steric hindrance, causing the three peripheral carboxyl groups to be perpendicular to the central benzene ring. This unique configuration allows the ligand to connect with the 8-connected Zr_6O_4 clusters, resulting in the formation of the first known Zr-MOF with the *the-a* topology (Fig. 1d) [53]. Interestingly, by employing formic acid as the modulating agent and DMF as the solvent, Bumstead et al. have documented the structure of the doubly interpenetrated phase of BUT-12, STA-26(Zr) [54–56]. Given the unique positions of these methyl groups, we anticipate that converting them to carboxylic groups will not alter the structure of the MOFs. As a result, a significant number of uncoordinated carboxylic groups can be incorporated into the MOF pores, giving it great potential in U(VI) capture. The ligand, 5'-(4-carboxyphenyl)-[1,1':3',1'-terphenyl]-2',4,4',6'-pentacarboxylic acid ($\text{H}_3\text{CTTA-3COOH}$), was successfully synthesized using H_3CTTA as the starting material through a one-step oxidation reaction in a nitric acid aqueous solution at 180°C , and its reaction with ZrOCl_2 successfully yielded the carboxylated MOF, $\text{Zr}_6\text{O}_4(\text{OH})_8(\text{H}_2\text{O})_4(\text{CTTA-3COOH})_{8/3}$ (BUT-12-3COOH). BUT-12-3COOH represents good chemical stability, high surface areas, as well as high density of uncoordinated carboxylic groups (6.93 mmol/g). BUT-12-3COOH demonstrates an impressive maximum sorption capacity of 235 mg/g for UO_2^{2+} ions, achieving equilibrium within a period of 360 min. Moreover, the potential practical applicability of BUT-12-3COOH for the treatment of actual radioactive wastewater has been validated via dynamic sorption experiments. Furthermore, the interaction between UO_2^{2+} and the structural framework of BUT-12-3COOH has been substantiated through comprehensive analyses utilizing techniques such as energy-dispersive X-ray spectroscopy (EDS), Fourier-transform infrared spectroscopy (FT-IR), and X-ray photoelectron spectroscopy (XPS) analysis.

2. Experimental section

2.1. Synthesis

The detailed description of the synthesis of the ligand, H_3CTTA -

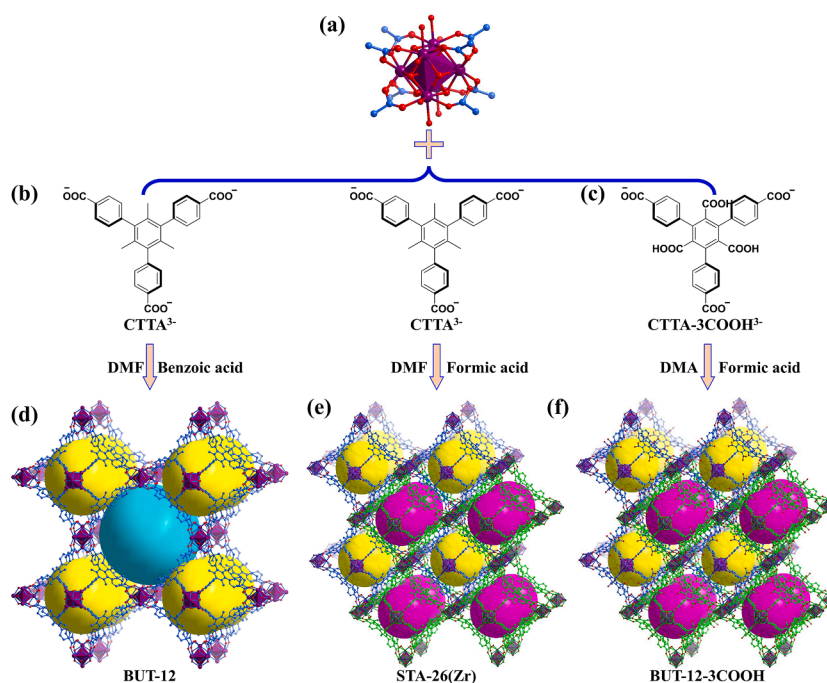


Fig. 1. (a) $\text{Zr}_6\text{O}_4(\text{OH})_8(\text{H}_2\text{O})_4(\text{COO})_8$ cluster; (b) CTTA^{3-} ligand; (c) CTTA-3COOH^{3-} ligand; framework structure of (d) BUT-12, (e) STA-26(Zr) and (f) BUT-12-3COOH (H atoms are omitted for clarity. color code: Zr, violet; C, light blue; and O, red). (For interpretation of the references to color in this figure legend, the reader is referred to the web version of this article.)

3COOH, is provided in section 4 of the Supporting Information.

2.1.1. $[\text{Zr}_6\text{O}_4(\text{OH})_8(\text{H}_2\text{O})_4(\text{CTTA-3COOH})_{8/3}]$ (BUT-12-3COOH)

$\text{H}_3\text{CTTA-3COOH}$ (60 mg, 0.11 mmol), $\text{ZrOCl}_2 \cdot 8\text{H}_2\text{O}$ (64 mg, 0.20 mmol), and formic acid (4 mL) were combined and ultrasonically dissolved in 8 mL of *N,N*-dimethylacetamide (DMA) within a 20 mL Pyrex vial, which was then securely sealed. This mixture was subjected to heating at 120 °C for 72 h in an oven. Upon cooling to ambient temperature, the resultant yellow crystals were collected via filtration, followed by sequential washing with DMA and acetone. The crystals were then left to dry in an open-air environment, yielding 32 mg of the product.

2.2. Adsorption experiments

The details of uranium sorption experiments were described in Supporting Information.

3. Results and discussion

3.1. Synthesis, structure, and characterization

Solvothermal reactions of $\text{H}_3\text{CTTA-3COOH}$ with $\text{ZrOCl}_2 \cdot 8\text{H}_2\text{O}$ in the presence of formic acid as the competing reagent in *N,N*-dimethylacetamide (DMA) at 120 °C yielded cubic-shaped single crystals of $\text{Zr}_6\text{O}_4(\text{OH})_8(\text{H}_2\text{O})_4(\text{CTTA-3COOH})_{8/3}$ (BUT-12-3COOH). Single-crystal X-ray diffraction (SCXRD) analysis reveals that BUT-12-3COOH exhibits a 2-fold interpenetrated framework structure (Fig. 1f). Structurally, one individual framework within BUT-12-3COOH comprises

classical $[\text{Zr}_6\text{O}_4(\text{OH})_8(\text{H}_2\text{O})_4(\text{CO}_2)_8]$ clusters, along with CTTA-3COOH^{3-} ligands (Fig. 1c,f). The Zr(IV) atoms in the cluster exhibit an eight-coordinate environment, with each Zr atom coordinated to eight O atoms, adopting a tetragonal antiprismatic coordination geometry (Fig. 1a). The arrangement of six clusters, combined with the coverage of eight CTTA-3COOH^{3-} linkers, leads to the formation of an octahedral cage capable of enclosing a sphere with a diameter of approximately 16 Å (Fig. S3d). These octahedral cages are intricately packed, resulting in the formation of a larger cavity that can accommodate a sphere with a diameter of approximately 27 Å (Fig. S3e). From the topological perspective, the CTTA-3COOH^{3-} ligand can be seen as a 3-connected node (Fig. S3a) and the Zr_6 cluster serves as an 8-connected node (Fig. S3b), the 3D structure of BUT-12-3COOH can thus be simplified as a 3,8-c binodal net, which corresponds to the *the-a* topology (Fig. S3f). Importantly, two identical frameworks intricately interpenetrate, with the second framework effectively filling the mesopores within the single framework. This results in the formation of the BUT-12-3COOH structure, where only the smaller octahedral cages are accessible (Fig. 1f). The total solvent-accessible volumes in frameworks of BUT-12-3COOH is estimated to be 55.6 % of its unit-cell volume, as estimated by PLATON[57]. It should be noted that the free carboxylic group density in BUT-12-3COOH is 6.93 mmol/g, which exceeds that of UiO-66-COOH (1.83 mmol/g) and UiO-66-2COOH (3.57 mmol/g).

The phase purity of the bulky sample was assessed through the measurement of powder X-ray diffraction (PXRD), which revealed a close resemblance between the experimental PXRD pattern and that obtained from the single-crystal data, providing compelling evidence of the exceptional phase purity of the bulky sample (Fig. 2a). The successful functionalization of linker with carboxylic groups was further

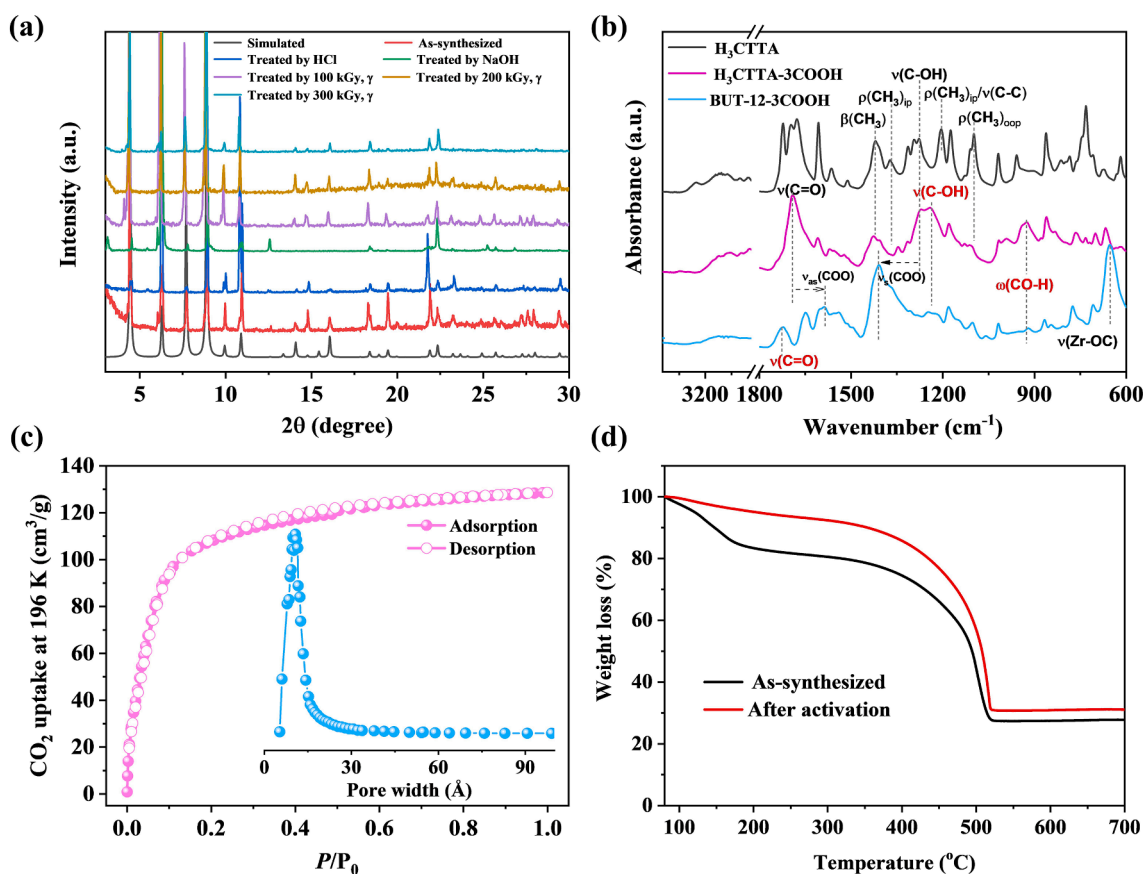


Fig. 2. (a) PXRD patterns of BUT-12-3COOH; (b) FT-IR spectra of BUT-12-3COOH and the ligands, H_3CTTA and $\text{H}_3\text{CTTA-3COOH}$, notation and acronym: ν = stretching, β = bending, ρ = rocking, ω = wagging, ip = in-plane, oop = out-of-plane, as = asymmetric, and s = symmetric; (c) CO_2 adsorption/desorption isotherms at 196 K of BUT-12-3COOH (inset shows pore size distribution evaluated by using the CO_2 adsorption data); (d) TGA curves of BUT-12-3COOH before and after activation.

confirmed by comparing the infrared spectra of the ligands H₃CTTA, H₃CTTA-3COOH and BUT-12-3COOH which reveals important changes associated with characteristic bands of methyl and carboxylic groups (Fig. 2b). Specifically, the in-plane/out-of-plan rocking (ρ) and bending (β) and modes of $-\text{CH}_3$ [58,59] disappear in the spectrum of H₃CTTA-3COOH. The resulting COOH after oxidation is best characterized by its strong $\nu(\text{C-OH})$ absorption at 1245 cm^{-1} , and broad $\omega(\text{CO-H})$ band at 1692 cm^{-1} [60] (see red label in Fig. 2b). In addition, an increased band at 1692 cm^{-1} can be ascribed to $\nu(\text{C}=\text{O})$ mode, which overlaps with peripheral $-\text{COOH}$ absorption. Upon forming MOF structure, the peripheral $-\text{COOH}$ groups underwent deprotonation and coordinated with the metal centers, as indicated by the loss of $\nu(\text{C}=\text{O})$ and $\nu(\text{C-OH})$, and the appearance of $\nu_{\text{as}}(\text{COO})$, $\nu_{\text{s}}(\text{COO})$ and $\nu(\text{Zr-OC})$ bands, which are located at 1585 , 1409 and 655 cm^{-1} respectively. The positions are determined based on the former studies of carboxylate groups in MOFs [61]. The functionalized COOH group remains unprotonated as suggested by the persistence of its $\nu(\text{C-OH})$, $\omega(\text{CO-H})$ and $\nu(\text{C}=\text{O})$ bands. Note that $\nu(\text{C}=\text{O})$ band blue-shifts to 1722 cm^{-1} , closer to the typical value of free carboxylic acid, since the COOH is isolated in the MOF pore [60]. The CO₂ sorption experiment conducted at 196 K confirmed the permanent porosity of BUT-12-3COOH (Fig. 2c). It demonstrated a saturated CO₂ uptake of 128 cm^3 (STP) g^{-1} and the Brunauer-Emmett-Teller (BET) surface area is calculated to be $416\text{ m}^2\text{ g}^{-1}$. The pore size distribution analysis based on the CO₂ adsorption data, revealed the presence of a single type of pore within BUT-12-3COOH, with a diameter measuring approximately 11 \AA (see inset in Fig. 2c). BUT-12-3COOH exhibits comparable thermal stability to other Zr-MOFs, as evidenced by its thermogravimetric analysis (TGA) curves up to around $420\text{ }^\circ\text{C}$ (Fig. 2d). To assess the chemical stability of BUT-12-3COOH, the samples were subjected to immersion in a 1 M HCl aqueous solution and a NaOH aqueous solution with a pH value of 10 at ambient temperature. Following 24 h of immersion, the PXRD patterns revealed maintained crystallinity and unaltered structures, underscoring the material's remarkable stability (Fig. 2a). The weight loss after treatment by HCl (1

M) and NaOH (pH = 10) aqueous solution was found to be 5 % and 8 %, respectively. Furthermore, given the critical importance of irradiation stability in the context of radioactive nuclear wastewater treatment, we subsequently investigated the irradiation resistance of BUT-12-3COOH. As depicted in Fig. 2a, exposure to γ -radiation ranging from 100 to 300 kGy resulted in no discernible alterations in the PXRD pattern of BUT-12-3COOH, affirming its robustness against γ -ray irradiation. This remarkable chemical and radiation stability can be attributed to the robust Zr-O coordination bonds present in the MOF. In terms of its high density of free carboxylic groups, and excellent chemical and radiation stability, BUT-12-3COOH was explored for the application of uranium sorption from water. For comparison, we synthesized the double interpenetrated phase of BUT-12, STA-26(Zr), and evaluated its adsorption capabilities for U(VI) [54–56]. The PXRD pattern of the synthesized STA-26(Zr) is depicted in Fig. S4, where it is observed that the PXRD of the bulk-synthesized sample aligns well with that of STA-26(Zr)-C, confirming its successful synthesis.

3.2. Uranium(VI) sorption

3.2.1. Effect of pH

The behavior and forms of metal ions in solution are significantly influenced by the pH level. As depicted in Fig. 3a, this is notably true for U(VI). At lower pH values (pH ≤ 4.0), the free UO_2^{2+} cation is the predominant form of U(VI) in aqueous environments. Yet, with an increase in pH, U(VI) transitions into various multinuclear hydroxide complexes, such as $(\text{UO}_2)_3(\text{OH})_5^{5+}$, $(\text{UO}_2)_4(\text{OH})_7^+$, $(\text{UO}_2)_3(\text{OH})_7^-$, $\text{UO}_2(\text{OH})_3$, and $\text{UO}_2(\text{OH})_4^{2-}$, among others. This transformation in U(VI) species composition is expected to influence its adsorption characteristics. Consequently, we explored how the sorption efficiency of BUT-12-3COOH for U(VI) varies across different pH levels. To guarantee the presence of U(VI) predominantly as UO_2^{2+} , our experiments were confined to a pH range of 2–4. As illustrated in Fig. 3b, the adsorption capacity of BUT-12-3COOH for U(VI) exhibits a clear dependence on pH.

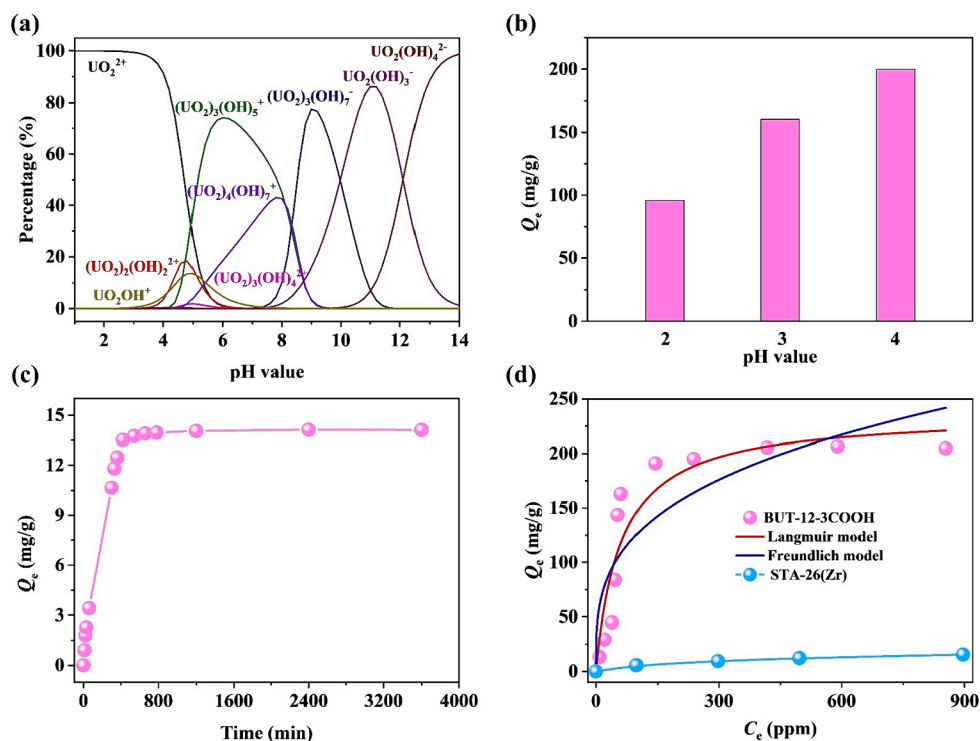


Fig. 3. (a) U(VI) speciation in aqueous solutions ($C_{\text{initial}} = 50\text{ ppm}$, $T = 298\text{ K}$, calculated by Visual MINTEQ 3.1); (b) Effect of pH on U(VI) sorption; (c) Sorption kinetics of U(VI) by BUT-12-3COOH. Condition: $[\text{U}]_{\text{initial}} = 10\text{ ppm}$ and $M_{\text{sorbent}}/V_{\text{solution}} = 0.25\text{ g/L}$. (d) Sorption isotherm of BUT-12-3COOH and STA-26(Zr) for U(VI) uptake. Condition: $M_{\text{sorbent}}/V_{\text{solution}} = 0.25\text{ g/L}$ and contact time = 12 h.

Specifically, within the pH window of 2–4, there is a consistent increase in the sorption capacity of BUT-12-3COOH for UO_2^{2+} . As the pH value increases from 2 to 4, the sorption capacity of BUT-12-3COOH towards UO_2^{2+} increases from 96 to 199 mg/g. This phenomenon is likely caused by changes in electrostatic interactions between the adsorbent and UO_2^{2+} in water. As the pH value increases, the uncoordinated carboxyl groups in the pores of BUT-12-3COOH lose protons and transform into $-\text{COO}^-$, thereby enhancing the electrostatic interactions with the positively charged UO_2^{2+} . Considering the high adsorption capacity and preventing excessive hydrolysis and precipitation of U(VI), a pH value of 4.0 was chosen for subsequent adsorption experiments.

3.2.2. Effect of contact time

For practical use, the time required to reach equilibrium is a key factor in assessing an adsorbent's viability. Thus, we conducted a study on the adsorption kinetics of U(VI) using BUT-12-3COOH as the sorbent. As shown in Fig. 3c, the adsorption of U(VI) on BUT-12-3COOH exhibited a rapid increase and eventually reached adsorption equilibrium within a span of 360 min. Although this equilibrium time is relatively slower compared to some MOF-based adsorbents such as UiO-66-AO[38] and MIL-101-NH₂[44], which achieved equilibrium in just 120 min, it still outperformed certain inorganic sorbents. For example, the time required to reach equilibrium for MCM-41[62] and carboxymethyl cellulose-grafted multiwalled carbon nanotubes[63] was 20 and 24 h, respectively. We employed both the pseudo-first-order and pseudo-second-order kinetic models to interpret the adsorption kinetics. The findings decisively demonstrate that the pseudo-second-order model exhibits significantly higher correlation coefficients (>99%) for U(VI) adsorption in BUT-12-3COOH. This strongly suggests that the adsorption process is governed by a chemical mechanism (Fig. S5 and Table S2).

3.2.3. Adsorption isotherm

Sorption capacity is a critical metric for assessing adsorbent performance. A higher removal capacity significantly enhances removal efficiency and helps minimize the production of secondary waste. We determined the sorption capacities for UO_2^{2+} on BUT-12-3COOH at equilibrium by varying the initial concentrations from 10 to 900 ppm, maintaining a material-to-solution ratio of 0.25 g/L. A reaction time of 12 h was chosen to ensure equilibrium was achieved. As shown in Fig. 3d, sorption of UO_2^{2+} by BUT-12-3COOH initially increases sharply at lower concentrations, then gradually plateaus as it nears the adsorbent's maximum capacity. The maximum sorption capacity of BUT-12-3COOH for UO_2^{2+} reached 235 mg/g, surpassing those of other carboxylic-functionalized MOFs, such as UiO-66-COOH (83 mg/g) and UiO-66-2COOH (189 mg/g) [47]. For comparison, the parent material, STA-26(Zr) exhibits no sorption ability toward UO_2^{2+} , highlighting the important role of the $-\text{COOH}$ group in the adsorption of UO_2^{2+} from water (Fig. 3d). To gain deeper insights into the adsorption mechanism, we employed both the Langmuir and Freundlich isotherm models for the analysis of our adsorption data. The analysis showed that the Langmuir model closely matches the adsorption behavior of U(VI) on BUT-12-3COOH (Fig. S6 and Table S4). This close match suggests that the adsorbent's surface is uniform and homogeneous. Moreover, it indicates the formation of a monolayer of U(VI) species on the surface of BUT-12-3COOH.

3.2.4. Dynamic sorption

To assess the sorption capabilities of BUT-12-3COOH in practical scenarios, we conducted dynamic sorption experiments using BUT-12-3COOH as the packing material (Fig. 4b). To create the experimental setup, we packed 200 mg of BUT-12-3COOH into a chromatographic column made from a 1 mL plastic syringe. Subsequently, a U(VI)

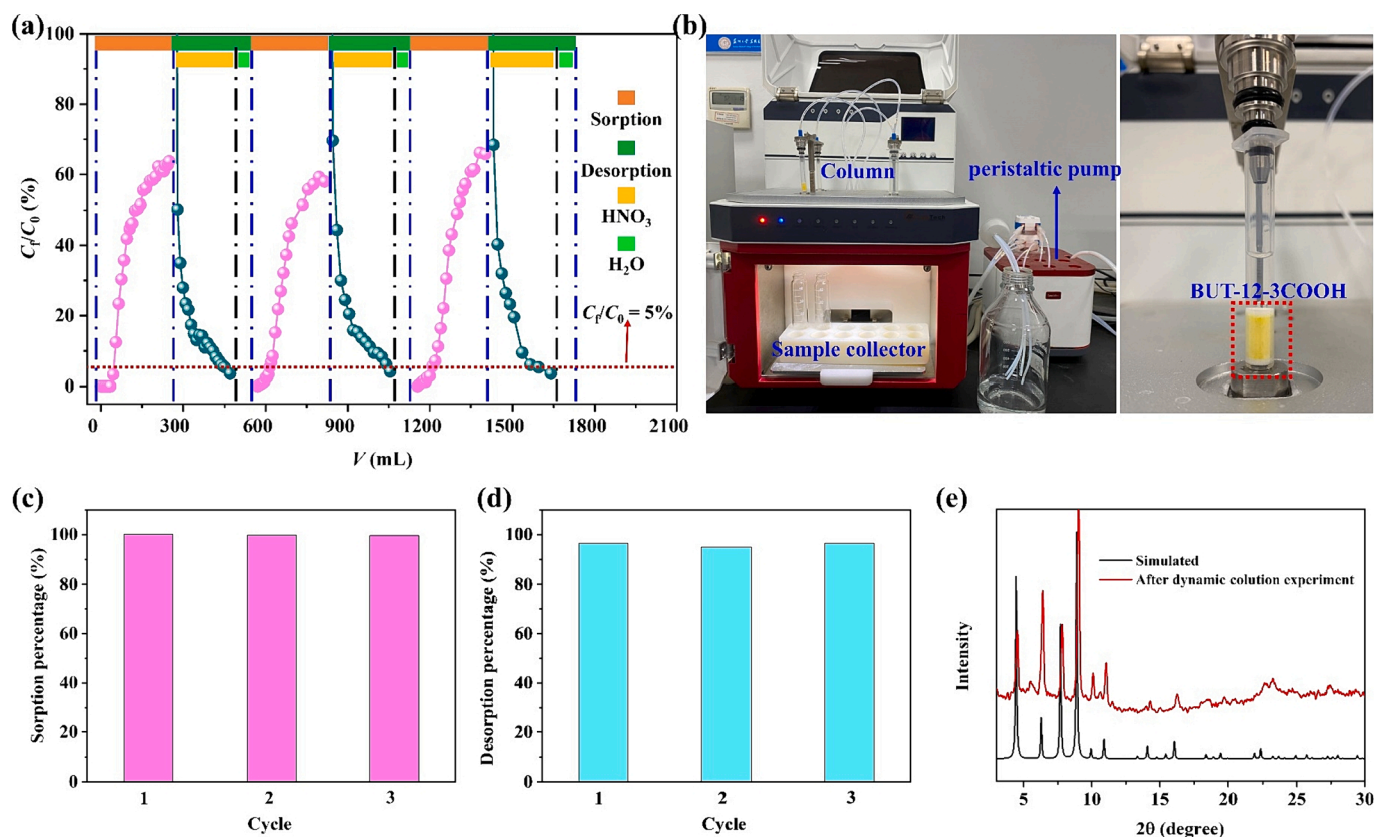


Fig. 4. (a) Dynamic elution curve showcasing U(VI) separation under the following conditions: initial U(VI) concentration = 10 ppm, sorbent mass = 200 mg, and flow rate = 3.0 mL/min; (b) Photograph of the dynamic adsorption apparatus (left) and the column (right) utilized in the experiments; (c) Sorption efficiency and (d) desorption efficiency for each cycle; (e) PXRD pattern of BUT-12-3COOH after dynamic column experiment.

aqueous solution with a concentration of 10 ppm was fed into the column at a flow rate of 3.0 mL/min. The effluent underwent analysis to determine the residual U(VI) concentration. The findings revealed a significant reduction in U(VI) concentration, with a residual concentration (C_f/C_0) of less than 5 % after processing 50 mL of the waste solution. As more solution was processed, the column quickly reached its saturation point, signifying that the maximum adsorption capacity of BUT-12-3COOH had been achieved (Fig. 4a). Remarkably, BUT-12-3COOH exhibited the capacity to treat a volume of U(VI) solution approximately 250 times greater than its own mass. After the sorption process, we washed and eluted the column using 40 mL of 0.05 M HNO_3 aqueous solution, followed by 100 mL of deionized water. As shown in Fig. 4a, the column can be fully regenerated. After three adsorption–desorption cycles, BUT-12-3COOH maintained its excellent adsorption performance. This can be ascribed to the structural stability of the MOF and reversible nature of its adsorption sites. Notably, across three dynamic cycles of adsorption–desorption, the system consistently maintained an adsorption efficiency greater than 99 % and a desorption efficiency exceeding 95 % in each cycle. In addition, after the dynamic sorption experiment, the crystallinity of BUT-12-3COOH remained well maintained, as evidenced by the PXRD measurement (Fig. 4e). These dynamic separation results highlight the exceptional potential of BUT-12-3COOH for practical applications in extracting U(VI) from radioactive waste.

3.2.5. Binding interaction

In order to understand the interaction between the uranyl ions and the adsorbents, we employed various techniques including EDS mapping, FT-IR, and XPS analysis. The EDS mapping images revealed that uranium is evenly distributed throughout BUT-12-3COOH (Fig. 5a and b). Fig. 5c showcases the FT-IR spectra for $\text{UO}_2(\text{NO}_2)_2$, BUT-12-3COOH@ UO_2^{2+} , and BUT-12-3COOH. The adsorption of UO_2^{2+} in BUT-12-3COOH@ UO_2^{2+} is clearly indicated by a unique band at 927 cm^{-1} . This band signifies the symmetric $\text{U}=\text{O}$ stretching vibration, aligning with observations from prior research [64]. Comparing the spectrum of $\text{UO}_2(\text{NO}_2)_2$, the peak center of the $\nu(\text{U}=\text{O})$ band in BUT-12-3COOH@ UO_2^{2+} shows a noticeable red shift of -10 cm^{-1} , indicating its favorable interaction with BUT-12-3COOH that softens the $\text{U}=\text{O}$ bond. The $\nu(\text{C}=\text{O})$ and $\nu(\text{C}-\text{OH})$ bands of BUT-12-3COOH also exhibit

significant red-shifts upon adsorbing UO_2^{2+} . These findings clearly suggest that UO_2^{2+} primarily interacts with the carboxylic groups of BUT-12-3COOH. XPS analysis was conducted to further investigate the adsorption site of UO_2^{2+} on BUT-12-3COOH. The presence of the U 4f signal in the survey spectrum of BUT-12-3COOH@ UO_2^{2+} confirms the existence of U(VI) oxidation state before and after adsorption (Fig. 5d). The peaks corresponding to U 4f_{7/2} and U 4f_{5/2} show a slight red-shift from 392.7 and 381.8 eV in the case of UO_2^{2+} to 392.5 and 381.6 eV in the case of BUT-12-3COOH@ UO_2^{2+} (Fig. 5e) [65]. This decrease in energy is indicative of the binding between uranyl and the carboxylic group functionalities, which serve as an electron donor [66]. Based on these findings, it can be inferred that BUT-12-3COOH exhibits strong binding with uranium. Similar phenomenon has been observed in our previously reported work [67].

4. Conclusions

In summary, we have successfully designed, synthesized, and utilized a novel and highly stable carboxylic group-functionalized Zr(IV)-based MOF named BUT-12-3COOH for the extraction of U(VI) from water. BUT-12-3COOH exhibits a maximum sorption capacity of 235 mg/g for UO_2^{2+} ions, and the sorption process reaches equilibrium within 360 min. Furthermore, we have demonstrated the potential of BUT-12-3COOH in treating real wastewater through dynamic sorption experiments. The binding between UO_2^{2+} and the framework of BUT-12-3COOH has been confirmed through DES, FT-IR, and XPS analysis. These findings highlight the great potential of BUT-12-3COOH for the extraction of U(VI) from radioactive wastewater.

CRediT authorship contribution statement

Bin Wang: Writing – original draft, Methodology, Investigation, Formal analysis, Data curation. **Chunyu Bao:** Investigation, Data curation. **Jiahui Xu:** Data curation, Investigation. **Yunnan Tao:** Investigation, Data curation. **Long Chen:** Investigation, Data curation. **Duo Zhang:** Investigation. **Kui Tan:** Formal analysis, Data curation. **Shuao Wang:** Resources, Project administration, Funding acquisition, Conceptualization. **Jian-Rong Li:** Funding acquisition, Conceptualization. **Shengqian Ma:** Writing – review & editing, Supervision,

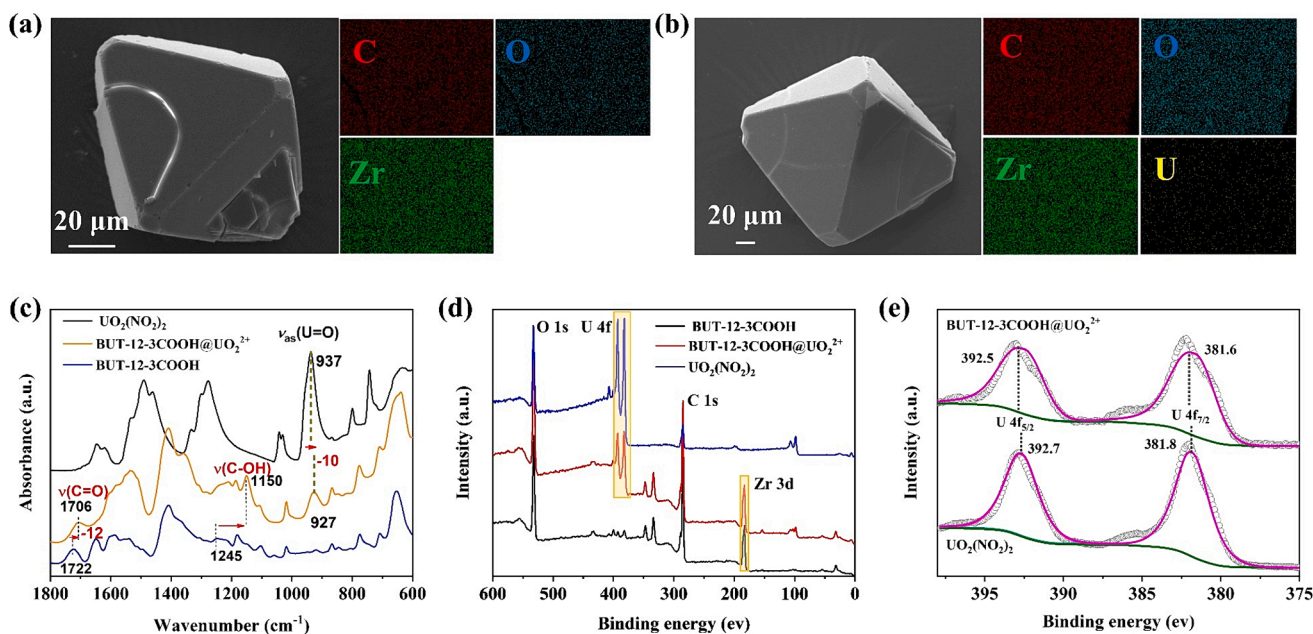


Fig. 5. SEM and EDS images of (a) BUT-12-3COOH and (b) BUT-12-3COOH@ UO_2^{2+} ; (c) FT-IR spectra and (d) XPS survey spectra of $\text{UO}_2(\text{NO}_2)_2$, BUT-12-3COOH@ UO_2^{2+} , and BUT-12-3COOH; (e) U 4f XPS spectra for $\text{UO}_2(\text{NO}_2)_2$ and BUT-12-3COOH@ UO_2^{2+} .

Resources, Project administration, Conceptualization.

Declaration of competing interest

The authors declare that they have no known competing financial interests or personal relationships that could have appeared to influence the work reported in this paper.

Data availability

Data will be made available on request.

Acknowledgment

Bin Wang, Chunyu Bao, and Jiahui Xu contributed equally to this work. The authors would like to thank the Robert A. Welch Foundation (B-0027) (S.M.) for its financial contribution to this research. Additionally, this study received partial funding from the National Natural Science Foundation of China (Grant Number 22227809).

Appendix A. Supplementary data

Supplementary data to this article can be found online at <https://doi.org/10.1016/j.cej.2024.150251>.

References

- [1] W.C. Patterson, *Nuclear power*, Penguin Books London, 1976.
- [2] <https://www.world-nuclear.org/our-association/publications/global-trends-reports/nuclear-fuel-report.aspx>.
- [3] D.S. Sholl, R.P. Lively, Seven chemical separations to change the world, *Nature* 532 (7600) (2016) 435–437, <https://doi.org/10.1038/532435a>.
- [4] C.W. Abney, R.T. Mayes, T. Saito, S. Dai, Materials for the recovery of uranium from seawater, *Chem. Rev.* 117 (23) (2017) 13935–14013, <https://doi.org/10.1021/acs.chemrev.7b00355>.
- [5] Y. Xie, Z. Liu, Y. Geng, H. Li, N. Wang, Y. Song, X. Wang, J. Chen, J. Wang, S. Ma, G. Ye, Uranium extraction from seawater: material design, emerging technologies and marine engineering, *Chem. Soc. Rev.* 52 (1) (2023) 97–162, <https://doi.org/10.1039/d2cs00595f>.
- [6] Y. Li, Y. Zheng, Z. Ahamd, L. Zhu, J. Yang, J. Chen, Z. Zhang, Strategies for designing highly efficient adsorbents to capture uranium from seawater, *Coord. Chem. Rev.* 491 (2023) 215234, <https://doi.org/10.1016/j.ccr.2023.215234>.
- [7] D. Mei, L. Liu, B. Yan, Adsorption of uranium (VI) by metal-organic frameworks and covalent-organic frameworks from water, *Coord. Chem. Rev.* 475 (2023) 214917, <https://doi.org/10.1016/j.ccr.2022.214917>.
- [8] Y. Wu, Y. Xie, X. Liu, Y. Li, J. Wang, Z. Chen, H. Yang, B. Hu, C. Shen, Z. Tang, Q. Huang, X. Wang, Functional nanomaterials for selective uranium recovery from seawater: material design, extraction properties and mechanisms, *Coord. Chem. Rev.* 483 (2023) 215097, <https://doi.org/10.1016/j.ccr.2023.215097>.
- [9] Y. Song, C. Zhu, Q. Sun, B. Aguilu, C.W. Abney, L. Wojtas, S. Ma, Nanospace decoration with uranyl-specific “hooks” for selective uranium extraction from seawater with ultrahigh enrichment index, *ACS Cent. Sci.* 7 (10) (2021) 1650–1656, <https://doi.org/10.1021/acscentsci.1c00906>.
- [10] H. Yang, X. Liu, M. Hao, Y. Xie, X. Wang, H. Tian, G.I.N. Waterhouse, P.E. Kruger, S.G. Telfer, S. Ma, Functionalized iron–nitrogen–carbon electrocatalyst provides a reversible electron transfer platform for efficient uranium extraction from seawater, *Adv. Mater.* 33 (51) (2021), <https://doi.org/10.1002/adma.202106621>.
- [11] X. Liu, Y. Xie, M. Hao, Z. Chen, H. Yang, G.I.N. Waterhouse, S. Ma, X. Wang, Highly efficient electrocatalytic uranium extraction from seawater over an amidoxime-functionalized In–N–C catalyst, *Adv. Sci.* 9 (23) (2022) 2201735, <https://doi.org/10.1002/advs.202201735>.
- [12] Q. Sun, Y. Song, B. Aguilu, A.S. Ivanov, V.S. Bryantsev, S. Ma, Spatial engineering direct cooperativity between binding sites for uranium sequestration, *Adv. Sci.* 8 (2) (2020) 2001573, <https://doi.org/10.1002/advs.202001573>.
- [13] H. Yang, M. Hao, Y. Xie, X. Liu, Y. Liu, Z. Chen, X. Wang, G.I.N. Waterhouse, S. Ma, Tuning local charge distribution in multicomponent covalent organic frameworks for dramatically enhanced photocatalytic uranium extraction, *Angew. Chem. Int. Ed.* 62 (30) (2023) e202303129, <https://doi.org/10.1002/anie.202303129>.
- [14] M. Hao, Z. Chen, X. Liu, X. Liu, J. Zhang, H. Yang, G.I.N. Waterhouse, X. Wang, S. Ma, Converging cooperative functions into the nanospace of covalent organic frameworks for efficient uranium extraction from seawater, *CCS Chem.* 4 (7) (2022) 2294–2307, <https://doi.org/10.31635/ccschem.022.202201897>.
- [15] A.S. Ivanov, B.F. Parker, Z. Zhang, B. Aguilu, Q. Sun, S. Ma, S. Jansone-Popova, J. Arnold, R.T. Mayes, S. Dai, V.S. Bryantsev, L. Rao, I. Popovs, Siderophore-inspired chelator hijacks uranium from aqueous medium, *Nat. Commun.* 10 (1) (2019) 819, <https://doi.org/10.1038/s41467-019-08758-1>.
- [16] Q. Sun, B. Aguilu, J. Perman, A.S. Ivanov, V.S. Bryantsev, L.D. Earl, C.W. Abney, L. Wojtas, S. Ma, Bio-inspired nano-traps for uranium extraction from seawater and recovery from nuclear waste, *Nat. Commun.* 9 (1) (2018) 91644, <https://doi.org/10.1038/s41467-018-04032-y>.
- [17] S.-M. Yi, C.-R. Zhang, X. Liu, X.-J. Chen, J.-X. Qi, C.-P. Niu, J.-L. Liu, R.-P. Liang, J.-D. Qiu, Efficient removal of uranium under strong acid based on charge separation and protonation coupled covalent organic frameworks, *Chem. Eng. J.* 475 (2023) 146264, <https://doi.org/10.1016/j.cej.2023.146264>.
- [18] M. Cao, Y. Wang, L. Feng, S. Zhao, H. Wang, T. Liu, Y. Yuan, N. Wang, Ion-imprinted nanocellulose aerogel with comprehensive optimized performance for uranium extraction from seawater, *Chem. Eng. J.* 475 (2023) 146048, <https://doi.org/10.1016/j.cej.2023.146048>.
- [19] F. He, Q. Xiao, Y. Chen, H. Wang, X. Wang, Synergistic reduction of U(VI) and selective oxidation of benzyl alcohol to prepare benzaldehyde via WO_x/g-C₃N₄, *Appl. Catal. B: Environ.* 343 (2024) 123525, <https://doi.org/10.1016/j.apcatb.2023.123525>.
- [20] Y. Li, L. Shi, Y. Mao, Y. Zhang, H. Wang, Efficient reduction of uranyl under aerobic conditions by sodium and potassium co-doped carbon nitride, *Chem. Eng. J.* 446 (2022) 136872, <https://doi.org/10.1016/j.cej.2022.136872>.
- [21] W. He, Z. Qiu, Q. Sun, Z. Li, Z. Chen, L. Hu, H. Wang, Amidoxime-functionalized hollow 2D-COFs for uranium separation, *Sep. Purif. Technol.* 331 (2024) 125620, <https://doi.org/10.1016/j.seppur.2023.125620>.
- [22] S. Wang, G. Wei, Y. Xie, H. Shang, Z. Chen, H. Wang, H. Yang, G.I.N. Waterhouse, X. Wang, Constructing nanotraps in covalent organic framework for uranium sequestration, *Sep. Purif. Technol.* 303 (2022) 122256, <https://doi.org/10.1016/j.seppur.2022.122256>.
- [23] M.P. Suh, H.J. Park, T.K. Prasad, D.-W. Lim, Hydrogen storage in metal–organic frameworks, *Chem. Rev.* 112 (2) (2012) 782–835.
- [24] K. Sumida, D.L. Rogow, J.A. Mason, T.M. McDonald, E.D. Bloch, Z.R. Herm, T.-H. Bae, J.R. Long, Carbon dioxide capture in metal–organic frameworks, *Chem. Rev.* 112 (2) (2012) 724–781.
- [25] J.R. Li, J. Sculley, H.C. Zhou, Metal-organic frameworks for separations, *Chem. Rev.* 112 (2) (2012) 869–932, <https://doi.org/10.1021/cr200190s>.
- [26] A. Bavykina, N. Kolobov, I.S. Khan, J.A. Bau, A. Ramirez, J. Gascon, Metal–organic frameworks in heterogeneous catalysis: recent progress, new trends, and future perspectives, *Chem. Rev.* 120 (16) (2020) 8468–8535.
- [27] L. Zhu, X.-Q. Liu, H.-L. Jiang, L.-B. Sun, Metal–organic frameworks for heterogeneous basic catalysis, *Chem. Rev.* 117 (12) (2017) 8129–8176.
- [28] D.-W. Lim, H. Kitagawa, Proton transport in metal–organic frameworks, *Chem. Rev.* 120 (16) (2020) 8416–8467.
- [29] L.S. Xie, G. Skorupskii, M. Dincă, Electrically conductive metal–organic frameworks, *Chem. Rev.* 120 (16) (2020) 8536–8580.
- [30] J.B. DeCoste, G.W. Peterson, Metal–organic frameworks for air purification of toxic chemicals, *Chem. Rev.* 114 (11) (2014) 5695–5727.
- [31] T. Islamoglu, Z. Chen, M.C. Wasson, C.T. Buru, K.O. Kirlikovali, U. Afrin, M. R. Mian, O.K. Farha, Metal–organic frameworks against toxic chemicals, *Chem. Rev.* 120 (16) (2020) 8130–8160.
- [32] P.-L. Wang, L.-H. Xie, E.A. Joseph, J.-R. Li, X.-O. Su, H.-C. Zhou, Metal–organic frameworks for food safety, *Chem. Rev.* 119 (18) (2019) 10638–10690.
- [33] Y. Cui, Y. Yue, G. Qian, B. Chen, Luminescent functional metal–organic frameworks, *Chem. Rev.* 112 (2) (2012) 1126–1162.
- [34] W. Gong, Z. Chen, J. Dong, Y. Liu, Y. Cui, Chiral metal–organic frameworks, *Chem. Rev.* 122 (9) (2022) 9078–9144.
- [35] S.M. Cohen, Postsynthetic methods for the functionalization of metal–organic frameworks, *Chem. Rev.* 112 (2) (2012) 970–1000.
- [36] Z. Zhao, G. Cheng, Y. Zhang, B. Han, X. Wang, Metal-organic-framework based functional materials for uranium recovery: performance optimization and structure/functionality-activity relationships, *ChemPlusChem* 86 (8) (2021) 1177–1192, <https://doi.org/10.1002/cplu.202100315>.
- [37] J. Xiong, Y. Fan, F. Luo, Grafting functional groups in metal–organic frameworks for U(VI) sorption from aqueous solutions, *Dalton Trans.* 49 (36) (2020) 12536–12545, <https://doi.org/10.1039/d0dt02088e>.
- [38] L. Chen, Z. Bai, L. Zhu, L. Zhang, Y. Cai, Y. Li, W. Liu, Y. Wang, L. Chen, J. Diwu, J. Wang, Z. Chai, S. Wang, Ultrafast and efficient extraction of uranium from seawater using an amidoxime appended metal-organic framework, *ACS Appl. Mater. Inter.* 9 (38) (2017) 32446–32451, <https://doi.org/10.1021/acsaami.7b12396>.
- [39] J.-M. Liu, T. Liu, C.-C. Wang, X.-H. Yin, Z.-H. Xiong, Introduction of amidoxime groups into metal-organic frameworks to synthesize MIL-53(Al)-AO for enhanced U(VI) sorption, *J. Mol. Liq.* 242 (2017) 531–536, <https://doi.org/10.1016/j.molliq.2017.07.024>.
- [40] X. Qin, W. Yang, W. Yang, Y. Ma, M. Li, C. Chen, Q. Pan, Covalent modification of ZIF-90 for uranium adsorption from seawater, *Micropor. Mesopor. Mat.* 323 (2021) 111231, <https://doi.org/10.1016/j.micromeso.2021.111231>.
- [41] W.-W. Zhao, L.-H. Li, J.-Z. Liao, R.-P. Liang, A.-M. Song, F.-D. Zhang, H. Ke, J.-D. Qiu, Regenerable and stable biomimetic hydroxyl-modified metal-organic frameworks for targeted uranium capture, *Chem. Eng. J.* 433 (2022) 133787, <https://doi.org/10.1016/j.cej.2021.133787>.
- [42] W.W. Zhao, L.H. Li, J.Z. Liao, H. Ke, R.P. Liang, J.D. Qiu, Preparation, characterization, and application of stable naphthalenediimide-based metal-organic framework for cooperative capture low concentration uranium from wastewater, *Environ. Prog. Sustain. Energy* (2023), <https://doi.org/10.1002/ep.14296>.
- [43] F. Liu, S. Song, G. Cheng, W. Xiong, L. Shi, Y. Zhang, MIL-101(Cr) metal–organic framework functionalized with tetraethylenepentamine for potential removal of uranium (VI) from waste water, *Adsorp. Sci. Technol.* 36 (7–8) (2018) 1550–1567, <https://doi.org/10.1177/0263617418789516>.

- [44] Z.-Q. Bai, L.-Y. Yuan, L. Zhu, Z.-R. Liu, S.-Q. Chu, L.-R. Zheng, J. Zhang, Z.-F. Chai, W.-Q. Shi, Introduction of amino groups into acid-resistant MOFs for enhanced U(VI) sorption, *J. Mater. Chem. A* 3 (2) (2015) 525–534, <https://doi.org/10.1039/c4ta04878d>.
- [45] B.-C. Luo, L.-Y. Yuan, Z.-F. Chai, W.-Q. Shi, Q. Tang, U(VI) capture from aqueous solution by highly porous and stable MOFs: UiO-66 and its amine derivative, *J. Radioanal. Nucl. Chem.* 307 (1) (2015) 269–276, <https://doi.org/10.1007/s10967-015-4108-3>.
- [46] J.Y. Zhang, N. Zhang, L. Zhang, Y. Fang, W. Deng, M. Yu, Z. Wang, L. Li, X. Liu, J. Li, Adsorption of uranyl ions on amine-functionalized MIL-101(Cr) nanoparticles by a facile coordination-based post-synthetic strategy and X-ray absorption spectroscopy studies, *Sci. Rep.* 5 (2015) 13514, <https://doi.org/10.1038/srep13514>.
- [47] B. Zhao, L. Yuan, Y. Wang, T. Duan, W. Shi, Carboxylated UiO-66 tailored for U(VI) and EU(III) trapping: from batch adsorption to dynamic column separation, *ACS Appl. Mater. Inter.* 13 (14) (2021) 16300–16308, <https://doi.org/10.1021/acscami.1c00364>.
- [48] Y. Peng, Y. Zhang, Q. Tan, H. Huang, Bioinspired construction of uranium ion trap with abundant phosphate functional groups, *ACS Appl. Mater. Inter.* 13 (23) (2021) 27049–27056, <https://doi.org/10.1021/acscami.1c04892>.
- [49] J. De Decker, J. Rochette, J. De Clercq, J. Florek, P. Van Der Voort, Carbamoylmethylphosphine oxide-functionalized MIL-101(Cr) as highly selective uranium adsorbent, *Anal. Chem.* 89 (11) (2017) 5678–5682, <https://doi.org/10.1021/acs.analchem.7b00821>.
- [50] X. Fu, J. Liu, Z. Ren, S. Zhang, F. Xiao, G. Peng, Introduction of phosphate groups into metal-organic frameworks to synthesize MIL-101(Cr)-PMIDA for selective adsorption of U(VI), *J. Radioanal. Nucl. Chem.* 331 (2) (2022) 889–902, <https://doi.org/10.1007/s10967-021-08161-5>.
- [51] D. Rinsant, E. Andreiadis, M. Carboni, D. Meyer, Uranium extraction from sulfuric acid media with Zr-metal-organic frameworks, *Mater. Lett.* 253 (2019) 285–288, <https://doi.org/10.1016/j.matlet.2019.06.090>.
- [52] Y. Bai, Y.B. Dou, L.H. Xie, W. Rutledge, J.R. Li, H.C. Zhou, Zr-based metal-organic frameworks: design, synthesis, structure, and applications, *Chem. Soc. Rev.* 45 (8) (2016) 2327–2367, <https://doi.org/10.1039/c5cs00837a>.
- [53] B. Wang, X.L. Lv, D.W. Feng, L.H. Xie, J. Zhang, M. Li, Y.B. Xie, J.R. Li, H.C. Zhou, Highly stable Zr(IV)-based metal-organic frameworks for the detection and removal of antibiotics and organic explosives in water, *J. Am. Chem. Soc.* 138 (19) (2016) 6204–6216, <https://doi.org/10.1021/jacs.6b01663>.
- [54] S.L. Hanna, M. Barsoum, T.T. Debel, C.D. Malliakas, M.A. Gaidimas, J.G. Knapp, K.O. Kiriakoval, C.H. Hendon, V.P. Dravid, O.K. Farha, Mapping the complete reaction energy landscape of a metal-organic framework phase transformation, *ACS Mater. Lett.* 5 (9) (2023) 2518–2527, <https://doi.org/10.1021/acsmaterialslett.3c00598>.
- [55] A.M. Bumstead, D.B. Cordes, D.M. Dawson, K.K. Chakarova, M.Y. Mihaylov, C. L. Hobday, T. Düren, K.I. Hadjiivanov, A.M.Z. Slawin, S.E. Ashbrook, R.R. Prasad, P.A. Wright, Modulator-controlled synthesis of microporous STA-26, an interpenetrated 8,3-connected zirconium MOF with the *the-i* topology, and its reversible lattice shift, *Chem. Eur. J.* 24 (23) (2018) 6115–6126, <https://doi.org/10.1002/chem.201705136>.
- [56] L. Robison, X. Gong, A.M. Evans, F.A. Son, X. Wang, L.R. Redfern, M.C. Wasson, Z. H. Syed, Z. Chen, K.B. Idrees, T. Islamoglu, M. Delferro, W.R. Dichtel, F.-X. Coudert, N.C. Gianneschi, O.K. Farha, Transient catenation in a zirconium-based metal-organic framework and its effect on mechanical stability and sorption properties, *J. Am. Chem. Soc.* 143 (3) (2021) 1503–1512, <https://doi.org/10.1021/jacs.0c11266>.
- [57] A.L. Spek, Single-crystal structure validation with the program PLATON, *J. Appl. Crystallogr.* 36 (2003) 7–13, <https://doi.org/10.1107/s0021889802022112>.
- [58] E. Kose, A. Atac, M. Karabacak, P.B. Nagabalasubramanian, A.M. Asiri, S. Periandy, FT-IR and FT-Raman, NMR and UV spectroscopic investigation and hybrid computational (HF and DFT) analysis on the molecular structure of mesitylene, *Spectrochim. Acta A Mol. Biomol. Spectrosc.* 116 (2013) 622–634, <https://doi.org/10.1016/j.saa.2013.07.070>.
- [59] H.M. Badawi, A study of the molecular structure and vibrational spectra of 1,3-dichloro-2-propanol and 1,1,1-trichloro-2-methyl-2-propanol (chlorobutanol), *Spectrochim. Acta A Mol. Biomol. Spectrosc.* 87 (2012) 11–14, <https://doi.org/10.1016/j.saa.2011.10.025>.
- [60] B.C. Smith, *The C=O bond, part III: carboxylic acids*, *Spectroscopy* 33 (2018) 14–20.
- [61] K.I. Hadjiivanov, D.A. Panayotov, M.Y. Mihaylov, E.Z. Ivanova, K.K. Chakarova, S. M. Andonova, N.L. Drenchev, Power of infrared and Raman spectroscopies to characterize metal-organic frameworks and investigate their interaction with guest molecules, *Chem. Rev.* 121 (3) (2020) 1286–1424, <https://doi.org/10.1021/acs.chemrev.0c00487>.
- [62] K. Vidya, S.E. Dapurkar, P. Selvam, S.K. Badamali, N.M. Gupta, The entrapment of UO₂²⁺ in mesoporous MCM-41 and MCM-48 molecular sieves, *Micropor. Mesopor. Mat.* 50 (2–3) (2001) 173–179, [https://doi.org/10.1016/s1387-1811\(01\)00445-0](https://doi.org/10.1016/s1387-1811(01)00445-0).
- [63] D. Shao, Z. Jiang, X. Wang, J. Li, Y. Meng, Plasma induced grafting carboxymethyl cellulose on multiwalled carbon nanotubes for the removal of UO₂²⁺ from aqueous solution, *J. Phys. Chem. B* 113 (4) (2009) 860–864, <https://doi.org/10.1021/jp8091094>.
- [64] N. Koshino, M. Harada, M. Nogami, Y. Morita, T. Kikuchi, Y. Ikeda, A structural study on uranyl (VI) nitrate complexes with cyclic amides: N-n-butyl-2-pyrrolidone, N-cyclohexylmethyl-2-pyrrolidone, and 1,3-dimethyl-2-imidazolidone, *Inorganica Chim. Acta* 358 (6) (2005) 1857–1864, <https://doi.org/10.1016/j.ica.2004.12.036>.
- [65] S. Amayri, T. Arnold, T. Reich, H. Foerstendorf, G. Geipel, G. Bernhard, A. Massaneck, Spectroscopic characterization of the uranium carbonate andersonite Na₂Ca[UO₂(CO₃)₃]·6H₂O, *Environ. Sci. Technol.* 38 (22) (2004) 6032–6036, <https://doi.org/10.1021/es049417l>.
- [66] A.A. Mosquera, D. Horwat, A. Rashkovskiy, A. Kovalev, P. Miska, D. Wainstein, J. M. Albella, J.L. Endrino, Exciton and core-level electron confinement effects in transparent ZnO thin films, *Sci. Rep.* 3 (1) (2013) 1714, <https://doi.org/10.1038/srep01714>.
- [67] B. Aguila, Q. Sun, H. Cassady, C.W. Abney, B. Li, S. Ma, Design strategies to enhance amidoxime chelators for uranium recovery, *ACS Appl. Mater. Inter.* 11 (34) (2019) 30919–30926, <https://doi.org/10.1021/acscami.9b09532>.